Editors' Suggestion   Featured in Physics

High Density Loading and Collisional Loss of Laser-Cooled Molecules in an Optical Trap

Varun Jorapur[1,2] Thomas K. Langin,[2] Qian Wang,[2] Geoffrey Zheng,[2] and David DeMille[2]

[1]*Department of Physics, Yale University, New Haven, Connecticut 06511, USA*
[2]*Department of Physics, University of Chicago, Chicago, Illinois 60637, USA*

We report optical trapping of laser-cooled molecules at sufficient density to observe molecule-molecule collisions for the first time in a bulk gas. SrF molecules from a red-detuned magneto-optical trap (MOT) are compressed and cooled in a blue-detuned MOT. Roughly 30% of these molecules are loaded into an optical dipole trap with peak number density $n_0 \approx 3 \times 10^{10}$ cm^{-3} and temperature $T \approx 40$ µK. We observe two-body loss with rate coefficient $\beta = 2.7^{+1.2}_{-0.8} \times 10^{-10}$ cm^3 s^{-1}. Achieving this density and temperature opens a path to evaporative cooling towards quantum degeneracy of laser-cooled molecules.

Ultracold polar molecules, with their long-range dipolar interactions and rich internal structure, have emerged as a powerful platform for quantum information science, quantum simulation, and precision probes of fundamental physics [1–6]. Techniques to directly laser cool molecules have developed rapidly in the past decade, with molecular magneto-optical traps (MOTs) demonstrated for several diatomic [7–10] and polyatomic [11] species. Subsequent sub-Doppler gray molasses cooling to temperatures $\lesssim 50$ µK [10,12–14] has enabled loading of molecules into conservative optical dipole traps (ODTs) [14–18]. Bulk gases of laser-cooled molecules in ODTs have been demonstrated with peak number densities $n_0 \sim 10^9$ cm^{-3} and phase space densities (PSDs) $\Phi \sim 10^{-7}$ [14–18]. However, higher n_0 and Φ are needed to implement collisional (evaporative and/or sympathetic) cooling, which is likely needed to achieve quantum degeneracy in such systems.

Collisional cooling requires a sufficiently high rate of thermalizing (elastic) collisions [19,20]. However, experiments with trapped ultracold molecules typically see rapid loss due to inelastic molecule-molecule collisions. Loss mechanisms include chemical reactions and "sticky collisions," where long-lived collision complexes are formed, then lost from the trap by absorbing a trap light photon or by colliding with a third body [21–33]. Recent experiments with assembled bi-alkali molecules, at much lower temperatures ($\lesssim 900$ nK), have demonstrated evaporative cooling by suppressing inelastic collisions using microwaves [20,34–38] or static electric fields [39,40], while also enhancing the elastic collision rate.

For directly laser-cooled molecules, inelastic collisions have been reported between molecules and atoms in a magnetic trap [25,41], and between pairs of CaF molecules in tweezers [26], where subsequent microwave shielding was demonstrated [36]. These results indicate that evaporative cooling of directly laser-cooled molecules could be as effective as it is for bi-alkalis, if sufficient density for

rethermalizing collisions is reached. Thus far, however, bulk gases of directly laser-cooled molecules have been too dilute for either elastic or inelastic molecule-molecule collisions to be observed. There are two primary reasons for this. First, standard red-detuned molecular MOTs (red MOTs) have low molecule number ($N \lesssim 10^5$), due to inefficient slowing of the source molecular beam and low capture velocity of the MOT. Second, transfer efficiency from these red MOTs into ODTs is low (typically $\lesssim 5\%$) [14,18]. This is due to sub-Doppler heating from the type-II transitions ($N_g = 1 \rightarrow N_e = 0$, where $N_g\{N_e\}$ is the rotational angular momentum of the ground {excited} state) required to be driven for rotational closure of molecular optical cycling [42–44], limiting typical red-MOT radii to $\sigma \gtrsim 1$ mm and temperatures to $T \gtrsim 1$ mK [7–9,11,16,45]. The temperature can be reduced to $\lesssim 50$ µK by blue-detuned molasses [10,12–14], but this does not provide spatial compression.

This has led to interest in "blue-detuned" type-II MOTs (blue MOTs), which can exhibit sub-Doppler cooling while simultaneously maintaining strong confining forces. This was first demonstrated in Rb atoms [46] and recently shown to work for the specific case of YO (yttrium-monoxide) molecules [47]. Recently published numerical simulations [44] suggested a generic method to produce blue MOTs for a large class of laser-coolable molecules, which should enable efficient transfer of molecules from a MOT to an ODT.

In this Letter, we experimentally realize this novel, generic scheme to produce a blue-MOT of SrF molecules. With it we achieve $\sim 10^2$ gain in n_0 and $\sim 10^4$ gain in Φ compared to our red MOT. We load an ODT from this blue MOT with $\sim 30\%$ transfer efficiency, ~ 10x higher than from a red MOT [14,18]. With this high density in the ODT, we are able to observe inelastic molecule-molecule collisions that result in two-body loss; to our knowledge this is the first such observation in a bulk gas of directly laser-cooled molecules.
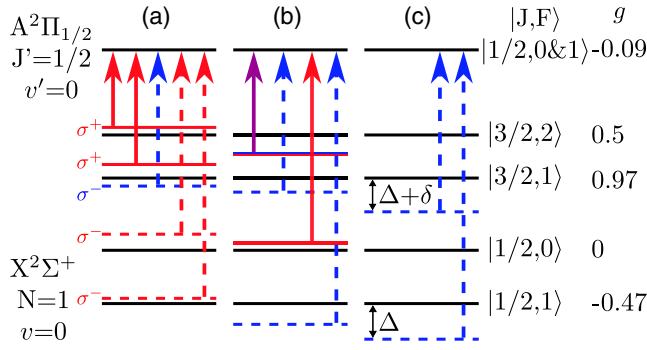
FIG. 1. Relevant SrF level structure and laser-driven transitions for different stages in the experiment, with hyperfine levels ($|J, F\rangle$) and their magnetic g factors (g) listed. Solid (dashed) lines indicate $\sigma^+ (\sigma^-)$ laser polarization, and color indicates red or blue detuning. (a) Red MOT, which employs the dual frequency mechanism on $|3/2, 1\rangle$. (b) Blue MOT, where the laser addressing $|3/2, 2\rangle$ is now blue, but also provides the red detuning needed for the dual frequency mechanism on $|3/2, 1\rangle$ (purple arrow). (c) Λ cooling, where only two lasers address $|3/2, 1\rangle$ and $|1/2, 1\rangle$.
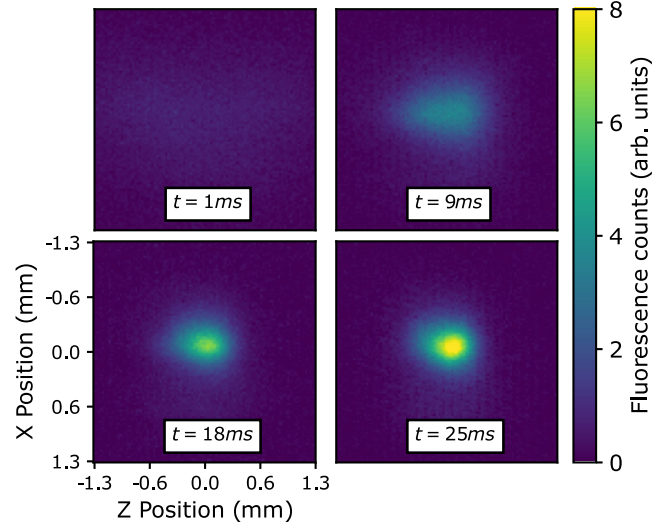

FIG. 2. Fluorescence images showing capture into the blue MOT (2 ms exposure starting at t after switching to the blue MOT). The loading is quick and efficient, with $\approx 80\%$ of molecules captured by $t = 30$ ms.

Our apparatus is very similar to that used in our prior work [18,48], but with several changes to improve the number of molecules captured in our MOT. We start with a cryogenic buffer gas beam source [48], where SrF molecules are produced by chemical reactions between laser ablated Sr and SF_6 gas. The molecules collide with cold (4 K) He gas and exit the cell at forward velocity ~ 130 m/s, then are slowed using the white light slowing technique [48,49] on the $X \to B$ transition for 14.5 ms.

Slowed molecules are captured in a direct current red MOT. Here, 3 hyperfine levels are addressed by solely red-detuned light, while simultaneous red- and blue-detuned light is applied on the $|J = 3/2, F = 1\rangle$ state [Fig. 1(a)] to create a dual-frequency trapping force [50]. Initially, the per-beam peak laser intensity is $I \sim 100$ mW/cm^2 (detailed intensity distribution in [51]) and the axial B-field gradient is $b = 16$ G/cm. After capturing the molecules, we linearly increase b to 29 G/cm and lower I to 10 mW/cm^2 over 30 ms. In this "compressed" MOT, the cloud radius (Gaussian rms width) is $\sigma \approx 1$ mm, with $T \approx 1$ mK and molecule number $N \approx 2.5 \times 10^4$. The value of N is determined by switching off the gradient and taking a fluorescence image (2 ms exposure) with $I \sim 170$ mW/cm^2, where the scattering rate is measured using the procedure from [7] and the detection efficiency is calibrated from offline measurements [53]. The fluorescence image is integrated along the radial direction, then fit to a 1D Gaussian plus constant offset; the fluorescence counts are extracted from the Gaussian integral. The temperature is measured using the time-of-flight (TOF) expansion method.

Next, we instantaneously jump to the blue-MOT configuration. The laser frequencies are changed to those in Fig. 1(b), and I is increased to ~ 170 mW/cm^2, corresponding to $I/I_{\text{sat}} \sim 60$, where I_{sat} is the saturation

intensity. As in the red MOT, a dual-frequency scheme is applied to the $|J = 3/2, F = 1\rangle$ state. However, blue-detuned light is applied to the other $F \neq 0$ states, resulting in simultaneous application of both sub-Doppler cooling and spatial confinement [44,46,47].

We find that $\sim 80\%$ of the molecules from the compressed red-MOT are captured by the blue MOT. Within 30 ms, the cloud radius is reduced to as low as $\sigma_{X,Z} \approx 150$ μm (here X, Z are the transverse and axial directions) and the temperature to as low as $T \approx 200$ μK (see Fig. 2), corresponding to peak density $n_0 \approx 4 \times 10^8$ cm^{-3}. The temperature can be lowered further to ≈ 60 μK by reducing I to 34 mW/cm^2, though this results in a larger transverse radius $\sigma_X \approx 230$ μm. The blue-MOT reaches a maximum PSD of $\Phi \approx 1.6 \times 10^{-9}$, $\sim 10^4$ larger than in the compressed red MOT.

We note that our trapping scheme is substantially different from that used for YO in Ref. [47], where only blue-detuned light was used. We were, by contrast, unable to observe trapping without employing a dual-frequency mechanism. We believe the difference lies in the fact that YO, unlike SrF, has a magnetically insensitive ground state $F = 1$ hyperfine manifold. This feature has been observed to increase the robustness of sub-Doppler cooling in magnetic fields [10]. The lack of this feature in SrF (and most other laser-cooled molecules) may necessitate the dual-frequency mechanism, which can provide stronger confining forces [44] at the cost of some heating. Indeed, we observe a stronger restoring force ($\sim 10\times$ faster compression) and smaller minimum cloud volume (by a factor of 2) at the cost of higher minimum blue-MOT temperature (60 vs 38 μK) compared to the pure-blue YO MOT [47].

Next, we load the ODT by switching the lasers to the Λ-enhanced gray molasses [14,18] configuration in Fig. 1(c),

and turning off the quadrupole field gradient. The ODT details are described elsewhere [18]; briefly, the ODT is formed from a 53 W, 1064 nm laser focused to a $1/e^2$ radius of 38 μm, with a trap depth $U_T \approx 1.3$ mK for SrF. Loading is optimized for two-photon detuning $\delta = 2\pi \times 0.11$ MHz, one-photon detuning $\Delta = 2\pi \times 22$ MHz, and $I \sim 57$ mW/cm². Owing to the small size of the blue MOT, the ODT is rapidly loaded, with up to 30% transfer efficiency achieved within 20 ms. This is an order of magnitude higher efficiency than achieved when loading from type-II red MOTs [14,18]. Under optimal conditions, we load an initial number $N_0 \approx 4000$ molecules in the ODT, at $T \approx 40$ μK and $n_0 \approx 3.4 \times 10^{10}$ cm⁻³. We note in passing that here, different from our previous observations, the optimal polarization of the ODT beam is linear and the temperature is higher [18]. We have been unable to trace the source of this change.

With these starting conditions, we look for evidence of inelastic molecule-molecule collisions by measuring the number of molecules remaining in the trap (N) as a function of the hold time (t_h). For all of these measurements, we load the ODT for 20 ms, then let untrapped molecules fall away by turning off the Λ-cooling light for 32 ms. This defines $t_h = 0$ and N_0. We then measure the remaining number at t_h, either by imaging *in situ* with Λ-cooling light (for points $t_h < 1$ s) [14], or by recapturing in the compressed red MOT and imaging (for points $t_h \geq 1$ s). The scattering rate for each method is determined by comparing the fluorescence counts to those from a free space image (2 ms exposure) at $I \sim 170$ mW/cm². We assign uncorrelated uncertainties to each $N(t_h)$ data point by adding in quadrature contributions from fit uncertainties, shot-to-shot fluctuations in the initial number, and uncertainties in the ratio of the extracted number between the two imaging methods [51].

First, we measure the loss rate in the maximally loaded ODT, with average initial number $N_0 \approx 4000$. We observe a fast initial loss, followed by a slow decay, as is characteristic of two-body loss processes (Fig. 3). The dynamics are modeled using the two-body loss rate equation, with evolution of the number density n given by

$$\dot{n} = -\frac{1}{\tau}n - \beta n^2, \qquad (1)$$

where τ is the one-body loss time constant and β is the two-body loss rate coefficient. To convert Eq. (1) to a number evolution, we assume a Gaussian spatial distribution and define an effective volume [$V_{\text{eff}} = (2\sqrt{\pi})^3 \sigma_x \sigma_y \sigma_z$] occupied by the molecules [27]; here z is the direction of propagation of the ODT beam, and x (y) is along the transverse direction in (perpendicular to) the imaging plane. This allows us to integrate over the volume to obtain

$$\dot{N} = -\frac{1}{\tau}N - \frac{\beta}{V_{\text{eff}}}N^2. \qquad (2)$$
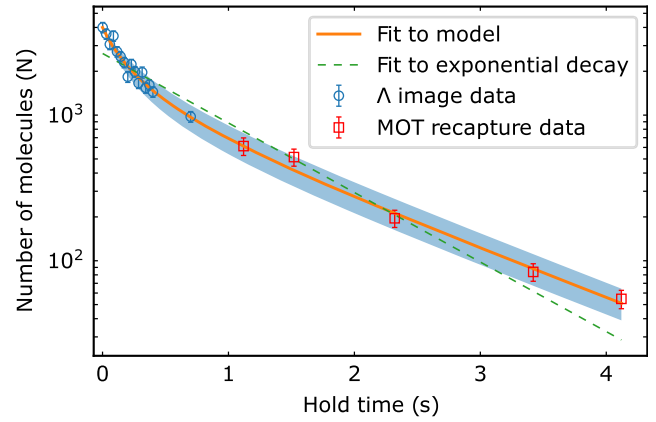

FIG. 3. Number of molecules in the trap as a function of hold time. Each point is an average of 15 images, and the error bars account for uncertainties as described in the main text. Data for $t_h < 1$ s are Λ images (blue circles) and the rest are MOT recapture images (red squares). The data show a clear deviation from an exponential decay, a classic signature of two-body loss. By fitting to a model where σ_z is increasing linearly with time, we extract a two-body loss rate coefficient $\beta = 2.7^{+1.2}_{-0.8} \times 10^{-10}$ cm³ s⁻¹, and a one-body loss time constant $\tau = 1.3(1)$ s. The shaded area indicates the uncertainty range.

If the spatial distribution is constant in time, Eq. (2) has an analytical solution:

$$N(t) = \frac{N_0}{\left(1 + \frac{\beta\tau N_0}{V_{\text{eff}}}\right)e^{t/\tau} - \frac{\beta N_0 \tau}{V_{\text{eff}}}}. \qquad (3)$$

Our imaging system cannot resolve σ_x and we cannot observe properties in the y direction. We do directly measure σ_z, as well as the temperatures T_x and T_z. We then infer σ_x using the calculated trap depth, measured ODT beam profile, and value of T_x [51], and assume $\sigma_y = \sigma_x$ by symmetry.

We observe that σ_z increases from its initial value linearly with hold time, and observe a corresponding increase in T_z. We attribute this to nonadiabatic dragging of the ODT trap center due to thermal lensing of the optics along the beam path [51]. However, we observe no change in T_x over time, so we assume that σ_x (and hence σ_y) does not change. To model this behavior, we treat V_{eff} as a function of time in Eq. (2), with σ_z increasing at the measured rate. We numerically integrate Eq. (2) to find values of β and τ that minimize the reduced chi squared (χ^2_{red}) of this model. With fixed $N_0 = 4000$, we find $\beta = 2.7(5) \times 10^{-10}$ cm³ s⁻¹ and $\tau = 1.3(1)$ s (with $\chi^2_{\text{red}} = 0.99$, see Fig. 3), where we incorporate the uncertainty in V_{eff} by adding it in quadrature to the uncertainty of the fit.

The final extracted value of β is strongly dependent on the initial number, so we also consider systematic uncertainties in determining N_0. The scattering rate is affected by uncertainty in the vibrational branching ratio $|A^2\Pi_{1/2}, v=0\rangle \rightarrow |X^2\Sigma, v=3\rangle$ [7,51,54], and in the calibration of

the imaging system. We estimate a combined uncertainty of 25% in N_0 [51]. We emphasize that this is different from shot-to-shot fluctuations, and instead is a correlated uncertainty for all points, which in turn leads to an uncertainty in the overall normalization of β. To determine the effect of this scale uncertainty, we use the same analysis method with initial numbers $N_0 = \{3000, 5000\}$, and numerically integrate Eq. (2) to find the optimal β for each N_0. The final uncertainty for β is then assigned as the quadrature sum of contributions from this systematic uncertainty and from the fit error for $N_0 = 4000$. Finally, we find $\beta = 2.7^{+1.2}_{-0.8} \times 10^{-10}$ cm^3 s^{-1} and $\tau = 1.3(1)$ s.

As a cross-check, we also fit the data to the analytical solution [Eq. (3)] by following the prescription from Ref. [37]. That is: we first extract $\tau = 1.2(2)$ s by fitting a pure exponential decay to only late-time ($t_h \geq 1$ s) data points. Then, we extract β by fixing τ and fitting only to early-time data points ($t_h < 250$ ms) where the axial radius change is small and V_{eff} can be treated as a constant; we use the average V_{eff} for $t_h < 250$ ms. With the same error analysis as before, we find $\beta = 2.7^{+1.4}_{-1.0} \times 10^{-10}$ cm^3 s^{-1} ($\chi^2_{\text{red}} = 1.20$), consistent with results from the more complete model.

To further verify the presence of density-dependent loss, we load the ODT with lower initial number (by using a shorter slowing pulse), $N_0 \approx 650$, but the same temperature and trap depth, thereby reducing the starting density by a factor of 6. We see that the short-time loss rate is reduced (Fig. 4). As expected, we find that the initial collision-induced loss rate is proportional to the initial density [51].

There are numerous possible loss channels in our experiment. The molecules are in the rotational $N = 1$ state, and rotational quenching to $N = 0$ can lead to large inelastic losses [41]. They also occupy all sublevels in the $N = 1$ manifold of hyperfine and spin-rotation states, opening up p- and f-wave collision channels that would be absent if all the (bosonic) molecules were in the same quantum state. In addition, colliding pairs of SrF molecules can undergo a barrierless chemical reaction [55], and "sticky collisions" between the molecules can also lead to losses [21–28].

We compare our measurement to theoretical and experimental benchmarks. The universal loss rate model [56], which assumes that colliding molecules are lost if they reach short range, i.e., if they do not reflect off the van der Waals (vdW) + centrifugal potential, has proven consistent with observed experimental loss rates [21–28,41]. We use the generic solutions from [57], which are valid for systems where the temperature (here, 40 μK) is above the p- and d-wave barriers (≈ 5 and ≈ 30 μK, respectively) determined by the C_6 coefficients for interactions between SrF molecules in an incoherent mixture of $N = 1$ sublevels. We find a thermally and ensemble-averaged loss rate constant $\beta_{\text{univ}} = 2.6 \times 10^{-10}$ cm^3 s^{-1}. We also calculate the maximum allowed loss rate constant by summing the maximum
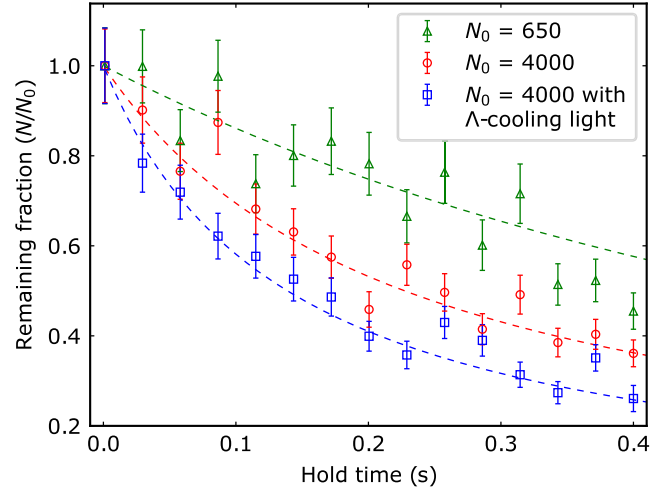

FIG. 4. Short-time evolution of trap population for different starting conditions. Dashed lines are fits for the first 9 points to the two body loss rate model with fixed $\tau = 1.3$ s and the average V_{eff} for $t_h < 250$ ms. Data with initial ODT number $N_0 \approx 650$ (green triangles) have a slower initial loss than for $N_0 \approx 4000$ (red circles), clearly demonstrating the density dependent loss. The presence of Λ-cooling light leads to additional two-body loss (blue squares) due to light-assisted collisions. For all conditions, the one-body loss rate remains the same (as seen in longer-time data, not shown).

inelastic cross-sections for each partial wave [58] and find $\beta_{\text{max}} = 2.8 \times 10^{-10}$ cm^3 s^{-1} [51,59]. The close match indicates small reflection probabilities, as expected for $T = 40$ μK. Our experimental measurement of β is consistent with both calculations.

The experiment which most closely matches ours is [5], in which pairs of CaF molecules in a mixture of $N = 1$ sublevels were held in optical tweezers at $T \approx 80$ μK, above (below) the p (d) wave barrier of 20 μK (100 μK). The reported loss rate constant was $\beta_{\text{CaF}} = 40 \times 10^{-10}$ cm^3 s^{-1}, $\sim 10\times$ larger than the predicted universal value, in contrast to our results, which match the model.

We also explore light-assisted collisions due to Λ cooling (Fig. 4). Here, we turn on the Λ-cooling light at $t_h = 0$. Though τ is unaffected, β increases to $\beta_{\text{tot}} = 4.9^{+1.7}_{-1.2} \times 10^{-10}$ cm^3 s^{-1} due to light-assisted collisions. This is two orders of magnitude lower than previously reported for CaF molecules held in optical tweezers [5]. Given the typical loading time (20 ms) from the blue-MOT, β_{tot} sets an upper bound, $n_0^{\text{max}} \sim 10^{11}$ cm^{-3}, on the peak density achievable by loading an ODT using Λ cooling. While the peak densities we achieve are lower than n_0^{max}, it may be possible to reach it if larger numbers of molecules [44], lower temperatures [15,18], and/or deeper traps can be achieved.

In conclusion, we have demonstrated high efficiency loading of a molecular gas into an ODT from a blue MOT and observed inelastic collisions in a bulk gas of directly laser-cooled molecules for the first time. Our results

suggest the possibility of using a shielding mechanism to enhance the elastic collision rate while suppressing two-body losses, as already used for evaporative cooling in experiments using assembled bi-alkali molecules [20,34–40]. Current efforts are underway to prepare the molecules in a single quantum state and to implement microwave shielding in our system. This will open a clear path to collisional cooling of directly laser-cooled molecules via evaporation or by sympathetic cooling with co-trapped atoms.

———

[1] D. DeMille, Quantum computation with trapped polar molecules, Phys. Rev. Lett. **88**, 067901 (2002).

[2] L. D. Carr, D. DeMille, R. V. Krems, and J. Ye, Cold and ultracold molecules: Science, technology and applications, New J. Phys. **11**, 055049 (2009).

[3] C. M. Holland, Y. Lu, and L. W. Cheuk, On-demand entanglement of molecules in a reconfigurable optical tweezer array, arXiv:2210.06309v1.

[4] Y. Bao, S. S. Yu, L. Anderegg, E. Chae, W. Ketterle, K. K. Ni, and J. M. Doyle, Dipolar spin-exchange and entanglement between molecules in an optical tweezer array, arXiv:2211.09780v1.

[5] L. Anderegg, L. W. Cheuk, Y. Bao, S. Burchesky, W. Ketterle, K. K. Ni, and J. M. Doyle, An optical tweezer array of ultracold molecules, Science **365**, 1156 (2019).

[6] T. S. Roussy, L. Caldwell, T. Wright, W. B. Cairncross, Y. Shagam, K. B. Ng, N. Scholssberger, S. Y. Park, A. Wang, J. Ye, and E. A. Cornell, A new bound on the electron's electric dipole moment, Science **381**, 46 (2023).

[7] E. B. Norrgard, D. J. McCarron, M. H. Steinecker, M. R. Tarbutt, and D. DeMille, Submillikelvin dipolar molecules in a radio-frequency magneto-optical trap, Phys. Rev. Lett. **116**, 063004 (2016).

[8] S. Truppe, H. J. Williams, M. Hambach, L. Caldwell, N. J. Fitch, E. A. Hinds, B. E. Sauer, and M. R. Tarbutt, Molecules cooled below the Doppler limit, Nat. Phys. **13**, 1173 (2017).

[9] L. Anderegg, B. L. Augenbraun, E. Chae, B. Hemmerling, N. R. Hutzler, A. Ravi, A. Collopy, J. Ye, W. Ketterle, and J. M. Doyle, Radio frequency magneto-optical trapping of CaF with high density, Phys. Rev. Lett. **119**, 103201 (2017).

[10] S. Ding, Y. Wu, I. A. Finneran, J. J. Burau, and J. Ye, Sub-Doppler cooling and compressed trapping of YO molecules at μK temperatures, Phys. Rev. X **10**, 021049 (2020).

[11] N. B. Vilas, C. Hallas, L. Anderegg, P. Robichaud, A. Winnicki, D. Mitra, and J. M. Doyle, Magneto-optical trapping and sub-Doppler cooling of a polyatomic molecule, Nature (London) **606**, 70 (2022).

[12] L. Caldwell, J. A. Devlin, H. J. Williams, N. J. Fitch, E. A. Hinds, B. E. Sauer, and M. R. Tarbutt, Deep laser cooling and efficient magnetic compression of molecules, Phys. Rev. Lett. **123**, 033202 (2019).

[13] D. J. McCarron, M. H. Steinecker, Y. Zhu, and D. DeMille, Magnetic trapping of an ultracold gas of polar molecules, Phys. Rev. Lett. **121**, 013202 (2018).

[14] L. W. Cheuk, L. Anderegg, B. L. Augenbraun, Y. Bao, S. Burchesky, W. Ketterle, and J. M. Doyle, Λ-enhanced imaging of molecules in an optical trap, Phys. Rev. Lett. **121**, 083201 (2018).

[15] Y. Wu, J. J. Burau, K. Mehling, J. Ye, and S. Ding, High phase-space density of laser-cooled molecules in an optical lattice, Phys. Rev. Lett. **127**, 263201 (2021).

[16] Y. Lu, C. M. Holland, and L. W. Cheuk, Molecular laser cooling in a dynamically tunable repulsive optical trap, Phys. Rev. Lett. **128**, 213201 (2022).

[17] C. Hallas, N. B. Vilas, L. Anderegg, P. Robichaud, A. Winnicki, C. Zhang, L. Cheng, and J. M. Doyle, Optical trapping of a polyatomic molecule in an l-type parity doublet state, Phys. Rev. Lett. **130**, 153202 (2023).

[18] T. K. Langin, V. Jorapur, Y. Zhu, Q. Wang, and D. DeMille, Polarization enhanced deep optical dipole trapping of Λ-cooled polar molecules, Phys. Rev. Lett. **127**, 163201 (2021).

[19] M. H. Anderson, J. R. Ensher, M. R. Matthews, C. E. Wieman, and E. A. Cornell, Observation of Bose-Einstein condensation in a dilute atomic vapor, Science **269**, 198 (1995).

[20] A. Schindewolf, R. Bause, X. Chen, M. Duda, T. Karman, I. Bloch, and X. Luo, Evaporation of microwave-shielded polar molecules to quantum degeneracy, Nature (London) **607**, 677 (2022).

[21] P. D. Gregory, M. D. Frye, J. A. Blackmore, E. M. Bridge, R. Sawant, J. M. Hutson, and S. L. Cornish, Sticky collisions of ultracold RbCs molecules, Nat. Commun. **10**, 3104 (2019).

[22] J. He, X. Ye, J. Lin, M. Guo, G. Quéméner, and D. Wang, Observation of resonant dipolar collisions in ultracold ^{23}Na^{87}Rb rotational mixtures, Phys. Rev. Res. **3**, 013016 (2021).

[23] K. K. Voges, P. Gersema, M. Meyerzum Alten Borgloh, T. A. Schulze, T. Hartmann, A. Zenesini, and S. Ospelkaus, Ultracold gas of bosonic ^{23}Na^{39}K ground-state molecules, Phys. Rev. Lett. **125**, 083401 (2020).

[24] R. Bause, A. Christianen, A. Schindewolf, I. Bloch, and X. Luo, Ultracold sticky collisions: Theoretical and experimental status, J. Phys. Chem. **127**, 729 (2023).

[25] Y. Segev, M. Pitzer, M. Karpov, N. Akerman, J. Narevicius, and E. Narevicius, Collisions between cold molecules in a superconducting magnetic trap, Nature (London) **572**, 189 (2019).

[26] L. W. Cheuk, L. Anderegg, Y. Bao, S. Burchesky, S. S. Yu, W. Ketterle, K. K. Ni, and J. M. Doyle, Observation of collisions between two ultracold ground-state CaF molecules, Phys. Rev. Lett. **125**, 043401 (2020).

[27] T. Takekoshi, L. Reichsöllner, A. Schindewolf, J. M. Hutson, C. R. Le Sueur, O. Dulieu, F. Ferlaino, R. Grimm, and H. C. Nägerl, Ultracold dense samples of dipolar RbCs molecules in the rovibrational and hyperfine ground state, Phys. Rev. Lett. **113**, 205301 (2014).

[28] J. W. Park, S. A. Will, and M. W. Zwierlein, Ultracold dipolar gas of fermionic ^{23}Na^{40}K molecules in their absolute ground state, Phys. Rev. Lett. **114**, 205302 (2015).

[29] A. Christianen, M. W. Zwierlein, G. C. Groenenboom, and T. Karman, Photoinduced two-body loss of ultracold molecules, Phys. Rev. Lett. **123**, 123402 (2019).

[30] P. D. Gregory, J. A. Blackmore, S. L. Bromley, and S. L. Cornish, Loss of ultracold ^{87}Rb^{133}Cs molecules via optical

excitation of long-lived two-body collision complexes, Phys. Rev. Lett. **124,** 163402 (2020).

[31] Y. Liu, M.-G. Hu, M. A. Nichols, D. D. Grimes, T. Karman, H. Guo, and K. K. Ni, Photo-excitation of long-lived transient intermediates in ultracold reactions, Nat. Phys. **16,** 1132 (2020).

[32] R. Bause, A. Schindewolf, R. Tao, M. Duda, X. Y. Chen, G. Quéméner, T. Karman, A. Christianen, I. Bloch, and X. Y. Luo, Collisions of ultracold molecules in bright and dark optical dipole traps, Phys. Rev. Res. **3,** 033013 (2021).

[33] P. Gersema, K. K. Voges, M. Meyerzum Alten Borgloh, L. Koch, T. Hartmann, A. Zenesini, S. Ospelkaus, J. Lin, J. He, and D. Wang, Probing photoinduced two-body loss of ultracold nonreactive bosonic $^{23}Na^{87}Rb$ and $^{23}Na^{39}K$ molecules, Phys. Rev. Lett. **127,** 163401 (2021).

[34] T. Karman and J. M. Hutson, Microwave shielding of ultracold polar molecules, Phys. Rev. Lett. **121,** 163401 (2018).

[35] L. Lassabliere and G. Quemener, Controlling the scattering length of ultracold dipolar molecules, Phys. Rev. Lett. **121,** 163402 (2018).

[36] L. Anderegg, S. Burchesky, Y. Bao, S. Yu, T. Karman, E. Chae, K. K. Ni, W. Ketterle, and J. M. Doyle, Observation of microwave shielding of ultracold molecules, Science **373,** 779 (2021).

[37] J. Lin, G. Chen, M. Jin, Z. Shi, F. Deng, W. Zhang, G. Quéméner, T. Shi, S. Yi, and D. Wang, Microwave shielding of bosonic NaRb molecules, Phys. Rev. X **13,** 031032 (2023).

[38] N. Bigagli, C. Warner, W. Yuan, S. Zhang, I. Stevenson, T. Karman, and S. Will, Collisionally stable gas of bosonic dipolar ground state molecules, Nat. Phys. **19,** 1579 (2023).

[39] G. Quéméner and J. L. Bohn, Shielding $^2\Sigma$ ultracold dipolar molecular collisions with electric fields, Phys. Rev. A **93,** 012704 (2016).

[40] J. Li, W. G. Tobias, K. Matsuda, C. Miller, G. Valotlina, L. D. Marco, R. Wang, L. Lassabliere, G. Quemener, J. L. Bohn, and J. Ye, Tuning of dipolar interactions and evaporative cooling in a three-dimensional molecular quantum gas, Nat. Phys. **17,** 1144 (2021).

[41] S. Jurgilas, A. Chakraborty, C. J. H. Rich, L. Caldwell, H. J. Williams, N. J. Fitch, B. E. Sauer, M. D. Frye, J. M. Hutson, and M. R. Tarbutt, Collisions between ultracold molecules and atoms in a magnetic trap, Phys. Rev. Lett. **126,** 153401 (2021).

[42] J. A. Devlin and M. R. Tarbutt, Three-dimensional Doppler, polarization-gradient, and magneto-optical forces for atoms and molecules with dark states, New J. Phys. **18,** 123017 (2016).

[43] J. A. Devlin and M. R. Tarbutt, Laser cooling and magneto-optical trapping of molecules analyzed using optical Bloch equations and the Fokker-Planck-Kramers equation, Phys. Rev. A **98,** 063415 (2018).

[44] T. K. Langin and D. DeMille, Toward improved loading, cooling, and trapping of molecules in magneto-optical traps, New J. Phys. **25,** 043005 (2023).

[45] A. L. Collopy, S. Ding, Y. Wu, I. A. Finneran, L. Anderegg, B. L. Augenbraun, J. M. Doyle, and J. Ye, 3D magneto-optical trap of yttrium monoxide, Phys. Rev. Lett. **121,** 213201 (2018).

[46] K. N. Jarvis, J. A. Devlin, T. E. Wall, B. E. Sauer, and M. R. Tarbutt, Blue-detuned magneto-optical trap, Phys. Rev. Lett. **120,** 083201 (2018).

[47] J. J. Burau, P. Aggarwal, K. Mehling, and J. Ye, Blue-detuned magneto-optical trap of molecules, Phys. Rev. Lett. **130,** 193401 (2023).

[48] J. F. Barry, D. J. McCarron, E. B. Norrgard, M. H. Steinecker, and D. DeMille, Magneto-optical trapping of a diatomic molecule, Nature (London) **512,** 286 (2014).

[49] J. F. Barry, E. S. Shuman, E. B. Norrgard, and D. DeMille, Laser radiation pressure slowing of a molecular beam, Phys. Rev. Lett. **108,** 103002 (2012).

[50] M. R. Tarbutt and T. C. Steimle, Modeling magneto-optical trapping of CaF molecules, Phys. Rev. A **92,** 053401 (2015).

[51] See Supplemental Material at http://link.aps.org/supplemental/10.1103/PhysRevLett.132.163403, which includes Refs. [52], for information on the blue-MOT, the data taking procedure, and the calculation of the unitarity limit.

[52] G. Quéméner, J. L. Bohn, A. Petrov, and S. Kotochigova, Universalities in ultracold reactions of alkali-metal polar molecules, Phys. Rev. A **84,** 062703 (2011).

[53] J. F. Barry, Laser cooling and slowing of a diatomic molecule, Ph.D. thesis, Yale University, New Haven CT, 2013.

[54] NL-eEDM Collaboration, High accuracy theoretical investigations of CaF, SrF, and BaF and implications for laser-cooling, J. Chem. Phys. **151,** 034302 (2019).

[55] E. R. Meyer and J. L. Bohn, Chemical pathways in ultracold reactions of SrF molecules, Phys. Rev. A **83,** 032714 (2011).

[56] Z. Idziaszek and P. S. Julienne, Universal rate constants for reactive collisions of ultracold molecules, Phys. Rev. Lett. **104,** 113202 (2010).

[57] M. D. Frye, P. S. Julienne, and J. M. Hutson, Cold atomic and molecular collisions: Approaching the universal loss regime, New J. Phys. **17,** 045019 (2015).

[58] L. D. Landau and E. M. Lifshitz, *Quantum Mechanics (Non-Relativistic Theory)* (Butterworth-Heinemann, Oxford, 1981).

[59] M. Lepers and O. Dulieu, Long-range interactions between ultracold atoms and molecules, arXiv:1703.02833.